

# Determination of diminished thermal conductivity in silicon thin films using scanning thermoreflectance thermometry

Max S. Aubain and Prabhakar R. Bandaru<sup>a)</sup>

Department of Mechanical Engineering, Materials Science Program, University of California, San Diego, La Jolla, California 92093, USA

(Received 28 September 2010; accepted 23 November 2010; published online 20 December 2010)

The variation of optical reflectance from silicon thin films in response to a change in temperature, i.e., the thermoreflectance, was used to monitor heat conduction processes within the films and confirm reduction of their in-plane thermal conductivity with decreasing film thickness. The measurements were also fit to numerical solutions of the heat conduction equation through which it was found that observed conductivity values were consistent with predictions based on phonon dispersion and phonon-boundary scattering considerations. The methods used may have practical implications for monitoring heat dissipation in silicon-on-insulator based microdevices. © 2010 American Institute of Physics. [doi:10.1063/1.3527966]

The study of heat dissipation in silicon thin films is important for insight into the effects of reduced dimensionality in thermal energy transport<sup>1</sup> and also in many applications,<sup>2</sup> e.g., for use as the *device layer* in silicon-on-insulator (SOI) structures in microelectronics for larger circuit density and superior device performance<sup>3</sup> through reduced parasitic capacitances. The high refractive index contrast in SOI structures also enables wavelength-scale photonic integrated circuits.<sup>4</sup> However, device performance<sup>5</sup> could deteriorate due to poor heat dissipation from the diminished in-plane thermal conductivity,  $\kappa_{ip}$ , of the silicon thin films in addition to the low thermal conductivity,  $\kappa$ , of the buried oxide (BOX). To probe such issues, many methods have been developed, none of which are completely satisfactory. For example, intrinsic ambiguity in the  $\kappa$  values of the films, arise through use of resistance thermometry<sup>6,7</sup> or the  $3\omega$  method<sup>8,9</sup> due to electrical/thermal contact related issues. Consequently, noncontact optical methods, e.g., employing thermoreflectance<sup>10</sup> (TR), are desirable.

In this context, time domain TR (Ref. 11) has been previously used to investigate thermal conductivity related issues and is based on heating the surface transiently through laser pulses. The lateral span of the initially heated region is of the order of the laser wavelength,  $\sim 1-10 \mu\text{m}$  practically, while the transverse span would correspond to the optical skin depth,  $\sim 50 \text{ nm}$ . Such large aspect ratio ensures that the resultant cross-plane heat transport is one-dimensional and was modeled as such. Through a subsequent time resolved measurement of the reflected radiation intensity, the thermal diffusivity could be obtained. Since heat transport perpendicular to the film surface in SOI structures is generally constrained by the BOX, it would be instructive and necessary to also measure the in-plane  $\kappa$  of the thin films and is the topic examined in this paper. We then demonstrate and model a scanning TR method for the determination of the  $\kappa_{ip}$  of Si thin films with thicknesses in the range of  $\sim 68-258 \text{ nm}$ . We observed a drastic reduction in the  $\kappa_{ip}$  with decreasing thickness, which was understood through a consideration of the phonon dispersion in silicon in addition to phonon-boundary scattering.

For the fabrication of Si films of varying thickness, a SOI wafer (from SOITEC S.A., Bernin, France), with a top Si single crystal device layer, *p*-type and (100) oriented, of thickness  $258 \pm 0.5 \text{ nm}$ , a *buried oxide layer* thickness of  $1 \mu\text{m}$ , on a Si substrate of  $\sim 675 \mu\text{m}$  was chosen, Fig. 1(b). Reactive ion etching of the device layer was used for producing lower film thicknesses. Metal lines ( $8-90 \mu\text{m}$  wide and  $4-12 \text{ mm}$  long) comprising Cr (10 nm)/Au (200 nm) were then deposited by electron-beam evaporation on the surface and used for resistive heating of the films. With reference to the cross section of the sample, the  $\sim 8 \mu\text{m}$  heaters may behave more like point sources of heat while at larger widths,  $\sim 90 \mu\text{m}$ , the cross-plane heat flow would be probed.<sup>9</sup> Enunciating the principle of our measurement, a

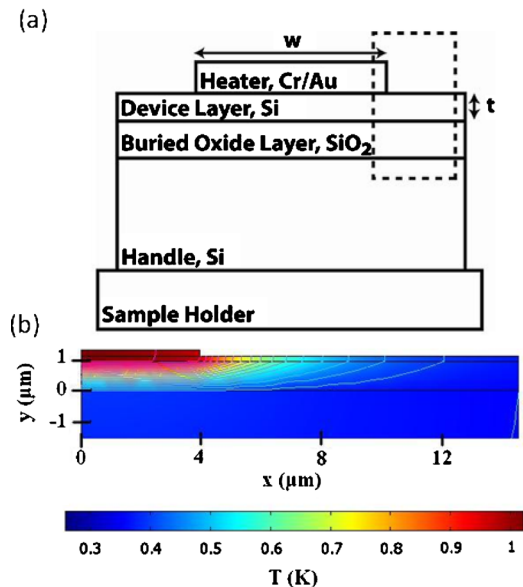


FIG. 1. (Color online) (a) Outline of experimental apparatus, for gauging the in-plane thermal conductivity ( $\kappa_{ip}$ ) of the Si thin films, through scanning thermoreflectance thermometry. (b) Schematic of the sample cross section, indicating the Si thin film device layer, BOX layer, and the underlying Si substrate (*handle*) with calculated temperature profile (from resistive heating through the Cr/Au metal lines) corresponding to the area in the dotted box. In the profile, the light blue contours indicate isotherms at each 0.05 K increment.

<sup>a)</sup>Electronic mail: pbandaru@ucsd.edu.

temperature change,  $\Delta T$ , due to the film heating would lead to a variation of the refractive index and consequently cause a change in the optical reflectance<sup>12</sup> at the interface. For small temperature variations, the relative reflectance change

$$\frac{\Delta R}{R} \sim \frac{1}{R} \frac{dR}{dT} \Delta T$$

can be monitored, as indicated through Fig. 1(a).

In the experiment, linearly polarized light from a He-Ne laser ( $\lambda=632.8$  nm, 10 mW) was circularly polarized by a quarter wave plate and focused normally to a spot radius of  $\sim 3$   $\mu\text{m}$  through a reflecting objective lens (Ealing, Rocklin, CA)  $36\times$ , Numerical Aperture=0.5, onto the device layer. The films were then heated by passing a sinusoidal current of frequency  $f$ , from a current source (6221: Keithley Instruments, Cleveland, OH), through the metal lines, which then produces a heating pulse at  $2f$  due to Joule heating. The heated sample was then scanned underneath the beam, away from the heater, while the reflected beam was diverted through a nonpolarized beam splitter. The reflected beam signal was transduced into a current by the photodetector DET110A, (from Thorlabs, Newton, NJ), subsequently amplified using a current preamplifier SR570 (from Stanford Research Systems, Sunnyvale, CA), and then measured through a lock-in amplifier (Stanford Research Systems SR830) tuned to the reference frequency of  $2f$ . The dynamic reserve of the lock-in amplifier was  $\sim 120$  dB and enables measurement up to the noise limit of the photodetector, yielding  $\Delta R/R$  to  $\sim 10^{-6}$ . The  $f$  was chosen to be  $\sim 2.5$  kHz, so that convective heating effects could be minimized and ignored. Additionally, an overall low measurement temperature mitigates radiative heat loss. At the chosen  $f$ , the thermal penetration depth<sup>13</sup> ( $=\sqrt{\kappa/2\pi f\rho C}$ , for a given density,  $\rho$ , and specific heat,  $C$ , of the sample) is  $\sim 75$   $\mu\text{m}$ , assuming bulk Si values ( $\kappa_{\text{Si}}=148$  W/m K,  $\rho_{\text{Si}}=2329$  kg/m<sup>3</sup>,  $C_{\text{Si}}\sim 1.67 \times 10^6$  J/m<sup>3</sup> K) and corresponds to heat spreading underneath the metal lines [see Fig. 1(b)]. This figure indicates results from a two-dimensional finite element model (COMSOL<sup>®</sup>, COMSOL, Inc., Los Angeles, CA) near the peak of the heating cycle, from the time-dependent temperature distribution along the sample cross section with incorporated parameters including the cross-plane thermal boundary conductance,  $h$ , input heating power,  $P$ , heating frequency,  $f$ , heater width,  $w$ , etc.

It was seen through such simulations that the largest temperature drop occurs over the BOX layer due to its low  $\kappa$  and that the thermal boundary resistance at the layer interfaces does not significantly modify heat flow. A representative, experimentally observed variation of the TR signal  $\Delta R/R$  along the surface of the silicon device layer is shown in Fig. 2. Each datum represents the averaged TR intensity over the width of the focused beam,  $\sim 6$   $\mu\text{m}$ , centered at the specified point. To evaluate the difference between the measured and actual temperature, a finite element model based distribution was used to find the *averaged temperature* over the width of the beam, which was compared to the *modeled temperature* at the center of the beam. The difference between the two values was found to be less than 2% implying that error due to the inherent averaging in the measurement was negligible. It was also obvious from such measured profiles that an exponential dependence, typical of one-dimensional heat flow,<sup>13</sup> would not exactly fit possibly due to

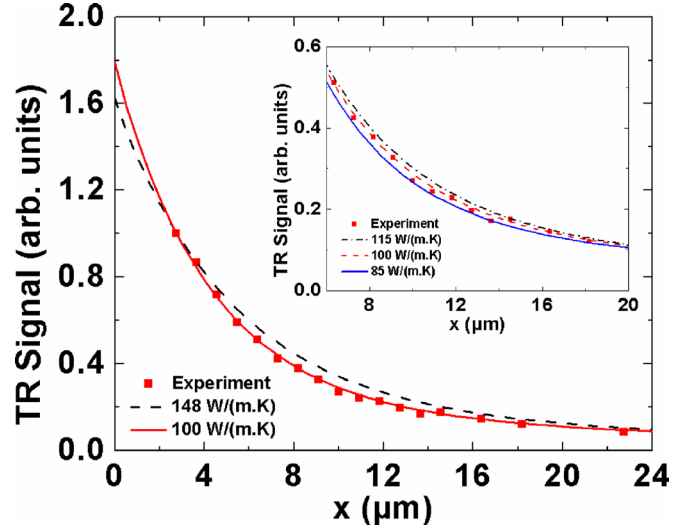


FIG. 2. (Color online) A typical normalized TR scan of a sample with a 235 nm device layer as a function of distance ( $x$ ) from the heater edge. Calculated fits of the in-plane thermal conductivity,  $\kappa_{ip}$ , comparing bulk ( $\sim 148$  W/m K) and predicted values ( $\sim 100$  W/m K) are shown. The inset shows a representative range of  $\kappa_{ip}$  that best fits data and approximately indicates the error ( $\pm 15$  W/m K) in the fitting of the  $\kappa$ .

cross-plane heat transfer in addition to lateral thermal transport along the device layer.

A quantitative determination of the  $\kappa_{ip}$  for the silicon device layer requires a robust correlation between the measured  $\Delta R$  and calculated  $\Delta T$ . At  $\lambda=633$  nm, the electromagnetic skin depth is  $\sim 2.29$   $\mu\text{m}$  (given that the complex index of refraction, at room temperature, for Si and SiO<sub>2</sub> is  $=3.92+0.022i$  and  $=1.457$ , respectively)<sup>14</sup> and implies that the light probe penetrates both the device and the BOX layers. The contribution to  $\Delta R$  would then arise from a modified reflectance due to a temperature induced refractive index change ( $d\tilde{n}/dT$ ) of the individual layers, i.e., considering both Si,<sup>15</sup>  $\sim (4.5+0.73i) \times 10^{-4}$  K<sup>-1</sup>, and amorphous<sup>16</sup> SiO<sub>2</sub>,  $\sim 10^{-5}$  K<sup>-1</sup>. An appropriate optical transfer function<sup>17</sup> was then constructed to model the total  $\Delta R$ .

It was seen through such modeling that the temperature variation of reflectance for the oxide layer could be orders of magnitude smaller compared to that for the silicon device layer, through dependence on the device layer thickness, and could affect the  $\Delta R$ . From the modeled temperature profiles, it was seen that the air/Si and Si/SiO<sub>2</sub> interfaces are at approximately the same temperature while the SiO<sub>2</sub>/substrate interface was relatively less heated due to the intervening oxide. Considering such factors, the *measured* temperature profile of a sample with a 235 nm device layer was overlaid on the *modeled* temperature profiles, each of which were constructed through assuming a different device layer  $\kappa_{ip}$ , as shown in Fig. 2 and the *inset*. Each curve was again scaled to have identical values at the peak data points to provide a baseline for comparison and fitting based on the relative curve shape. The  $\kappa_{ip}$  was hence determined from measurements on device layer thicknesses in the 68–258 nm range and plotted in Fig. 3.

It was deduced from this figure that  $\kappa_{ip}$  is reduced drastically from the bulk value in the thin films. We have modeled such variation through the Boltzmann transport equation incorporating diffuse phonon-boundary scattering at the device layer/oxide and the device layer/air interfaces. Tradi-

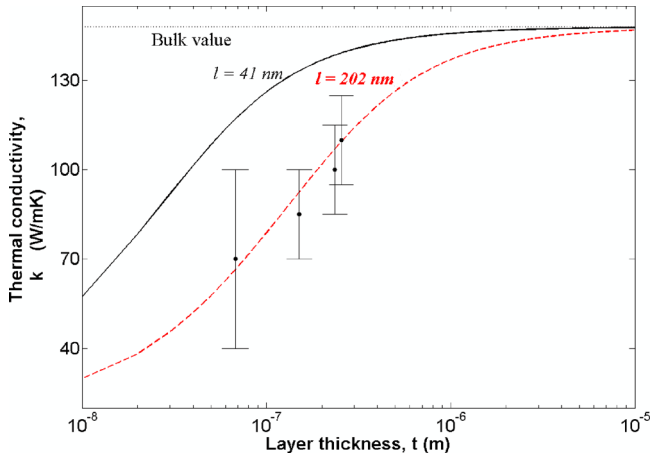


FIG. 3. (Color online) Predicted and measured in-plane thermal conductivity of the device layers of various thicknesses, corresponding to 68, 151, 235, and 258 nm in thickness. The  $l$  values of 41 and 202 nm refer to the phonon mean free paths in the *gray* approximation and through a consideration of phonon dispersion, respectively.

tional analysis assuming that all the phonons (both acoustic and optical) contribute to the thermal conductivity (the “gray” approximation<sup>18</sup>) typically yields a mean free path ( $l_{\text{mfp}}$ ) of  $\sim 41$  nm (using the bulk values of the specific heat capacity,  $C_{\text{Si}} \sim 1.67 \times 10^6$  J/m<sup>3</sup> K and sound velocity,  $v_{\text{Si}} \sim 6.4 \times 10^3$  m/s) and suggests a reduced  $\kappa$  for film thicknesses less than  $\sim 40$  nm. However, we considered, in addition to phonon-boundary scattering, (a) the complete phonon dispersion in silicon,<sup>19</sup> (b) that only the acoustic phonons contribute, while the optical phonons do not contribute due to their small group velocity, and (c) that the specific heat capacity and velocity would be those appropriate for acoustic phonons, i.e.,  $C'_{\text{Si}} \sim 0.95 \times 10^6$  J/m<sup>3</sup> K and  $v'_{\text{Si}} \sim 2.3 \times 10^3$  m/s. We then deduced a modified  $l_{\text{mfp}}$  of  $\sim 200$  nm, with an implication of a reduced  $\kappa_{\text{ip}}$  at film thicknesses in this regime. The results of such modeling are indicated as dashed lines in Fig. 3, where good agreement of the experimental data with the modified  $l_{\text{mfp}}$  was observed.

In summary, we have shown that the determination of optical reflectance from thin silicon layers could be used to gauge their in-plane thermal conductivity and understand lateral thermal energy transport. The accordance of experimental results with numerical simulations and theoretical models validates the proposed methodology.

We gratefully acknowledge support from the National Science Foundation (Grant No. ECS 0643761). The assistance of B. Fruhberger and R. Anderson at the Nano3 facility at UC, San Diego and discussions with A. Arriagada, M. Gollner, and R. Mifflin are appreciated.

- <sup>1</sup>D. G. Cahill, K. E. Goodson, and A. Majumdar, *J. Heat Transfer* **124**, 223 (2002).
- <sup>2</sup>S. M. Sze and K. K. Ng, *Physics of Semiconductor Devices* (Wiley, Hoboken, NJ, 2006).
- <sup>3</sup>Y. Taur, D. A. Buchanan, W. Chen, D. J. Frank, K. E. Ismail, S. Lo, G. A. Sai-Halasz, R. G. Viswanathan, H. C. Wann, S. J. Wind, and H. Wong, *Proc. IEEE* **85**, 486 (1997).
- <sup>4</sup>S. K. Selvaraja, P. Jaenen, W. Bogaerts, D. Van Thourhout, P. Dumon, and R. Baets, *J. Lightwave Technol.* **27**, 4076 (2009).
- <sup>5</sup>M. Asheghi, Y. K. Leung, S. S. Wong, and K. E. Goodson, *Appl. Phys. Lett.* **71**, 1798 (1997).
- <sup>6</sup>W. Liu and M. Asheghi, *J. Heat Transfer* **128**, 75 (2006).
- <sup>7</sup>Y. S. Ju and K. E. Goodson, *Appl. Phys. Lett.* **74**, 3005 (1999).
- <sup>8</sup>S.-M. Lee and D. G. Cahill, *J. Appl. Phys.* **81**, 2590 (1997).
- <sup>9</sup>T. Borca-Tasciuc, A. R. Kumar, and G. Chen, *Rev. Sci. Instrum.* **72**, 2139 (2001).
- <sup>10</sup>C. A. Paddock and G. L. Eesley, *J. Appl. Phys.* **60**, 285 (1986).
- <sup>11</sup>Y. K. Koh and D. G. Cahill, *Phys. Rev. B* **76**, 075207 (2007).
- <sup>12</sup>B. E. A. Saleh and M. C. Teich, *Fundamentals of Photonics*, 2nd ed. (Wiley, Hoboken, NJ, 2007).
- <sup>13</sup>H. S. Carslaw and J. C. Jaeger, *Conduction of Heat in Solids*, 2nd ed. (Oxford University Press, New York, 1986).
- <sup>14</sup>D. R. Lide, *CRC Handbook Chemistry and Physics*, 85th ed. (CRC Press, Boca Raton, FL, 2004).
- <sup>15</sup>G. E. Jellison and H. H. Burke, *J. Appl. Phys.* **60**, 841 (1986).
- <sup>16</sup>J. H. Wray and J. T. Neu, *J. Opt. Soc. Am. A* **59**, 774 (1969).
- <sup>17</sup>M. Born and E. Wolf, *Principles of Optics: Electromagnetic Theory of Propagation, Interference and Diffraction of Light* (Cambridge University Press, Cambridge, 1997).
- <sup>18</sup>G. Chen, *Nanoscale Energy Transport and Conversion* (Oxford University Press, New York, NY, 2005).
- <sup>19</sup>B. N. Brockhouse, *Phys. Rev. Lett.* **2**, 256 (1959).